Cum Laude Poster Award

Towards non-invasive electrocardiographic imaging using regularized neural networks

Abhejit Rajagopal, Vincent Radzicki, Hua Lee, and Shivkumar Chandrasekaran

Department of Electrical and Computer Engineering,
University of California, Santa Barbara, USA 93106

ABSTRACT

We present a new data-driven technique for non-invasive electronic imaging of cardiovascular tissues using routinely-measured body-surface electrocardiogram (ECG) signals. While traditional ECG imaging and 3D reconstruction algorithms typically rely on a combination of linear Fourier theory, geometric and parametric modeling, and invasive measurements via catheters, we show in this work that it is possible to learn the complicated inverse map, from body-surface potentials to epicardial or endocardial potentials, by exploiting the powerful approximation properties of neural networks. The key contribution here is a formulation of the inverse problem that allows historical data to be leveraged as ground-truth for training the inverse operator. We provide some initial experiments, and outline a path for extending this technique for real-time diagnostic applications.

Keywords: electrocardiographic imaging, inverse electromagnetic scattering, deep neural networks

1. INTRODUCTION

Although structural and/or functional abnormality of the cardiac electrovascular system is the most common cause of world mortality,[1] an affordable and inexpensive imaging modality for cardiac electrophysiology and arrhythmias does not yet exist in clinical practice. Instead, clinicians often rely on analysis of traditional electrocardiography signals (e.g. 12-lead ECG) to identify or diagnose abnormalities in the cardiac electrical system, and expensive CT, MRI, or invasive mapping techniques for quantifying and interrogating them. From a practical point of view, a non-invasive technique for compiling, correlating, and annotating externally-observable cardiac information is desirable, since it may enable clinicians to more quickly identify and localize the source of cardiac abnormalities prior to surgery, especially in facilities with limited characterization equipment.[2]

In this vein, the goal of electrocardiographic imaging (ECGI) is to create diagnostically relevant images of the electrophysiological processes in the heart from the electric signals measured on the body surface.[3] These images are useful in a number of medical applications, including mapping the mechanical and structural properties of the heart, identifying damaged or abnormal cardiovascular tissue, and monitoring or understanding the dynamics of heart function in various pathologies.[4] Currently available solution methods for this problem typically combine three types of information: (1) multiple simultaneous electrical measurements (typically anywhere from 6 to over 200), (2) a model of the electrical properties of the volume conductor between heart and torso (usually obtained via anatomical imaging such as CT or MRI and mild assumptions about electrical conductivity), and (3) a mathematical characterization of the electrical sources (as surface potential distributions surrounding the myocardium or distributed throughout the myocardial wall), or simplified models such as rotating charge or current dipoles with known waveforms but unknown time constants (e.g. activation or recovery time).[5]

While the electrical characterization of human tissue has been studied in some detail, and practitioners have a good idea of the expected material parameters to initialize the reconstructed geometry, utilizing these measurements has historically been both a numerical and algorithmic challenge. Practitioners are typically interested in anatomically-relevant models, but faithfully simulating such large and intricate 3D dielectric structures can quickly grow to be computationally intractable. Instead, practitioners have re-formulated various aspects of the problem to decrease this complexity, such as via boundary-element methods (as opposed to volume-elements),

Further author information: (Send correspondence to A.R.)
A.R.: E-mail: abhejit@ece.ucsb.edu, Telephone: 1 949 232 6195

Medical Imaging 2018: Physics of Medical Imaging, edited by Joseph Y. Lo, Taly Gilat Schmidt, Guang-Hong Chen, Proc. of SPIE Vol. 10573, 105732O
© 2018 SPIE · CCC code: 1605-7422/18/$18 · doi: 10.1117/12.2294474

Downloaded From: https://www.spiedigitallibrary.org/conference-proceedings-of-spie on 3/11/2018 Terms of Use: https://www.spiedigitallibrary.org/terms-of-use

structured-matrix representations, and fast eigenvalue solvers. Still, these approaches have practical limitations. For example, currently available modeling and reconstruction algorithms typically require time-consuming manual correlation, adjustment, and tuning by a domain expert, and are not suitable for time-critical applications such as surgery or on-site prognosis. Overwhelmingly, the reason for this is because the mathematical problem of recovering interior electronic potentials from surface measurements is inherently ill-posed, and "quasi"-solutions to this problem require a careful mathematical formulation that may be fragile to the integrity of pre-requisite input information (e.g. geometry, conductivity, and source distribution estimates).[6]

To address such concerns, in this paper we take a non-traditional approach to electrocardiographic imaging. We start with modeling the forward electromagnetic problem using some simplifying assumptions, and use this to derive an inversion or reconstruction algorithm. However, we quickly deviate from this linear formulation by allowing many of the constitutive parameters of the physical model to be "free", and tuned automatically using historical data from torso tank and invasive procedures, such as prior to or during ablation procedures. We further expand on this formulation by naturally introducing non-linear elements and computation structures that resemble the architectures of modern polynomial neural networks, which are used to increase the accuracy of the input-output map from body-surface potentials to epicardial potentials in a given patient. In particular, we emphasize that the structure of the resulting network is deliberate, and the resulting non-linear formulation was designed in-principle to overcome the simplifications used in the forward modeling stage. In the set of initial experiments presented in this paper, we demonstrate that neural networks are able to accurately estimate the voltage profile of the endocardium from body-surface measurements to within 312μV, or roughly 12.5% of the expected value, at any given time instant. This validates our hypothesis and suggests the feasibility of future modeling and optimization experiments that can extend such a scheme to cross-patient diagnostic applications.

The rest of the paper is organized as follows. In Section 2.1 we model the forward problem of electromagnetic simulation of the heart, and use this to motivate the quantities to be estimated in the inverse problem, discussed in Section 2.2. In particular, we use this intuition to develop a regularized neural-network-based reconstruction algorithm capable of leveraging historical data, and provide some initial results for our method on a free publicly-available dataset. Finally in Section 3 we discuss our findings, and indicate a path for both stabilizing the presented algorithms numerically and extending them for use in cross-patient clinical diagnostic applications.

2. METHODS

In this section, we outline a model of the forward electromagnetic problem and use this to derive a formulation of the inverse problem that can leverage historical data. In particular, our approach is aligned with classical Fourier imaging theory, but extends this approach using non-linear networks and gradient-based optimization.

2.1 Modeling of the Forward Problem

We begin with the time-dependent Maxwell's Equations:

$$\nabla \cdot B = 0 \tag{1}$$

$$\nabla \times H - \frac{dD}{dt} = J \tag{2}$$

$$\nabla \cdot D = \rho_v \tag{3}$$

$$\nabla \times E + \frac{dB}{dt} = 0 \tag{4}$$

Typically, at this point, an assumption of a dielectric model is introduced, which simplifies Maxwell's equations to a system of two variables. The most basic model (e.g. for linear isotropic media) is that the electric field is a linear function of the electric flux density (i.e. $D = \epsilon E$), with a similar but converse relationship governing the magnetic field (i.e. $B = \mu H$). While this considerably simplifies the formulation and derivation of the Helmholtz wave equation, we do not make this substitution immediately so that complications from non-linearities are clear. Using instead the substitutions $D = f(\epsilon, E)$ and $B = g(\mu, H)$, taking the curl of Equation 2 and Equation 4,

Downloaded From: https://www.spiedigitallibrary.org/conference-proceedings-of-spie on 3/11/2018 Terms of Use: https://www.spiedigitallibrary.org/terms-of-use

and assuming solutions with time harmonic time dependence $e^{j\omega t}$ from which we can build an arbitrary solution by Fourier superposition, yields the *coupled* relations:

$$0 = \nabla^2 \tilde{H} - \nabla(\nabla \cdot \tilde{H}) + (\nabla \times \tilde{J}) + (j\omega)(\nabla \times \tilde{f}(\epsilon, E)) \tag{5}$$

$$0 = \nabla^2 \tilde{E} - \nabla(\nabla \cdot \tilde{E}) + (-j\omega)(\nabla \times \tilde{g}(\mu, H)) \tag{6}$$

That is, the Helmholtz wave equation does not follow naturally from Maxwell's equations in the most general case of non-linear inhomogenous anisotropic media (i.e. the most general case). However, in a number of cases this system of equations can simplify. For example, in *linear inhomogeneous* media, we can reduce Eq. 5 and 6 using the divergence relations (Eq. 1 and 3) to the vector wave equation:

$$\nabla^2 \tilde{E} + \frac{\omega^2}{c^2}\tilde{E} = \frac{1}{\epsilon}\nabla \rho_v + j\omega\mu\tilde{J} \tag{7}$$

$$\nabla^2 \tilde{B} + \frac{\omega^2}{c^2}\tilde{B} = \mu(\nabla \times \tilde{J}) \tag{8}$$

This system further simplifies when the directional components of the electric and magnetic field are assumed to be uncoupled; that is, the off-diagonal entries of the local constitutive parameter tensors (ϵ and μ) are assumed to be 0. Further, when there are no static or flowing charges in the domain, the electric and magnetic fields themselves are uncoupled, and this system reduces exactly to the Helmholtz equation:

$$\nabla^2 A + k^2 A = 0 \tag{9}$$

using the substitution $k = \frac{\omega}{c}$, and noting that the equation is identical for $A = \tilde{E}$ and $A = \tilde{B}$. The Helmholtz equation has analytic solutions, commonly formulated using spherical Bessel functions, and is the basis of classical Fourier imaging theory. For reference the work of Nenonen et al. provides some practical bio-domain models of the torso,[7] while the work of Macovski provides a good overview of the physics-based formulation.[8]

In particular, to model the imaging problem, classical formulations adopt a modified version of the Helmholtz equation, known as the "inhomogeneous" Helmholtz equation, which lumps the terms on the right-hand side of Eq. 7 and 8 into a single forcing function $f(x)$ of compact support (Eq. 10).

$$\nabla^2 A(x) + k^2 A(x) = f(x) \tag{10}$$

In order to solve this equation uniquely, a boundary condition must be specified; a typical choice for this is the Sommerfeld radiation condition, which indicates that the scattered wavefield amplitude should approach zero at infinity, a point typically outside the domain of interest. With this condition, the solution to the inhomogeneous Helmholtz equation, $A(x)$, is given by the convolution:

$$A(x) = (G * f)(x) = \int_{\Omega} G(x - y) f(y) \delta y \tag{11}$$

where the forcing term $f(x)$ has compact support (i.e. an initial excitation), and $G(x)$ is the Green's function of the media. The Green's function can be found by solving the inhomogeneous Helmholtz equation for a Dirac delta input ($f(x) = -\delta(x)$), and is known to be dependent on the dimension of the input space. For example, in 3-dimensional problems involving a single medium, the Green's function is of the form:

$$G(x) = \frac{e^{jk|x|}}{4\pi|x|} \tag{12}$$

which can be understood as a spherically symmetric wave. In short, the Green's kernel, summarizes the effect of a linear directionally-uncoupled medium on an incident wavefield pattern, and can be used to model the forward and reverse propagation of electromagnetic waves in a homogeneous medium, such as the human torso.

Downloaded From: https://www.spiedigitallibrary.org/conference-proceedings-of-spie on 3/11/2018 Terms of Use: https://www.spiedigitallibrary.org/terms-of-use

2.2 Modeling of the Inverse Problem

In many cases, the Green's function formulation of the solution to the previously described Helmholtz equation affords a simple algebraic structure, which can be expressed with the relation:

$$Gx = b \tag{13}$$

where in this case G is the Green's kernel constructed from Eq. 12 by incorporating the torso and cardiac electrode geometry, b is the measured wavefield data on the torso, and x is the unknown source-wavefield or cardiac potentials to be predicted. As such, the least-squares solution can be written down as:

$$\hat{x} \approx (G^H G)^{-1} G^H b \tag{14}$$

although in practice there are many numerical and computational issues with computing this quantity directly. For example, in general G is an infinite-dimensional operator, so computing and inverting $G^H G$ can be both costly and numerically unstable. While in practice a simplification is typically made to instead compute the estimate $\hat{x}$ using the adjoint-operator, we do not emphasize this here. Instead, we assume the existence of some pseudo-inverse operator $G^\dagger$, and allow these parameters to be free variables which we solve for in the "training" phase of our algorithm. For example, this can be done by introducing a new term L, as:

$$\hat{x} \approx L G^H b \tag{15}$$

In the imaging literature, this reconstruction algorithm is known as filtered back-projection, and is a popular tool because it affords a simple and fast solution to the inverse problem. However, there are many issues that must be addressed in order to apply this algorithm to electrocardiographic imaging. Most pressing of these issues is that, at modest sampling frequencies ($\leq$ 10kHz) and dielectrics $\epsilon_r \leq 100$, the Green's kernel G is nearly a uniform matrix with extremely low spatial bandwidth. In effect, the direct application of G^H diffuses measured wavefield data, producing very poor spatial resolution in the reconstruction. In fact, this has historically been the limiting factor in applying Fourier imaging theory to relatively low-frequency measurements, such as ECG, with theoretical results requiring operating frequencies orders of magnitude higher than what is typically measured.

In this paper we argue that, through the systematic introduction of multiple algebraic terms, we can turn the reconstruction and estimation task into a non-linear problem that can overcome some of the limitations posed by linear Fourier theory. That is, if we view filtered back-projection or any variant reconstruction algorithm as a non-linear neural network that can be optimized, it may be possible to accurately reconstruct interior electronic potentials solely from non-invasive body-surface potentials, providing an algorithmic solution to the classic inverse problem of electrocardiographic imaging that is compatible with current hardware systems.

To see this, we first note that Eq. 15 resembles a 2-layer fully-connected neural network, albeit without a non-linear activation. Still, if we consider a given entry of $\hat{x}$, we see that:

$$\hat{x}_k = \sum_j^n \sum_i^m (L_{k,j} \cdot G_{j,i}) \cdot b_i \tag{16}$$

where $x \in \mathcal{C}^n$, $b \in \mathcal{C}^m$, $L \in \mathcal{C}^{n,n}$, and $G \in \mathcal{C}^{n,m}$ in the general case, although real-valued versions are possible. In this formulation, we see that allowing the parameters in G^H to be free results in a multi-variable non-linear problem, which could admit solutions that result in highly accurate predictions of the epicardial potential from body-surface measurements, beyond the capability of what would be possible using only a single free variable.

Moreover, we expand on this formulation by naturally introducing additional non-linearities in the network, in a fashion similar to the construction of modern deep neural networks and polynomial networks. For example, in our experiments, we found the following network structure outperforms the simple 2-layer structure on the

Downloaded From: https://www.spiedigitallibrary.org/conference-proceedings-of-spie on 3/11/2018 Terms of Use: https://www.spiedigitallibrary.org/terms-of-use

sample dataset used (discussed in Section 3):

$$a_0 = b \tag{17}$$

$$a_1 = G^H \cdot a_0 \tag{18}$$

$$a_2 = L \cdot a_1 \tag{19}$$

$$a_3 = a_2 + c \tag{20}$$

$$\hat{x} = a_4 = w_0 + w_1 a_3 + w_2 + a_3^2 + w_3 a_3^3 \tag{21}$$

where the newly introduced variables are $c, w_0, w_1, w_2, w_3 \in \mathcal{R}^n$, and the for the k-th entry of $\hat{x}$ we may write:

$$\hat{x}_k = \sum_{p=1}^{3} w_{p,k} \Big(\big(\sum_{j}^{n} \sum_{i}^{m} (L_{k,j} \cdot G_{j,i}) \cdot b_i \big) + c_k \Big)^p \tag{22}$$

That is, Equations 17-21 define the network structure, and Equation 22 defines the computation required for reconstruction or prediction of the potential at a spatial point corresponding to the k-th electrode.

While in theory, this network could be used for estimation of dense 3D potential profiles, in practice we are limited to comparing the accuracy of the estimation at known electrode locations. Accordingly, to train our algorithm we compare the network output $\hat{x}$ with the ground-truth electrode value, denoted as x, using a simple 2-norm metric that we include in our objective function as:

$$\hat{\omega} = \min_{\omega} ||x - \hat{x}||_2 \tag{23}$$

where ω denotes the collection of trainable variables and weights used to compute the network output, including L, G, c, and polynomial weights w_p.

In this initial study, we did not investigate special routines for training these network structures, and instead relied on gradient-based methods such as gradient descent with line-search. However, we note that we did initialize these algorithms with intelligent choices for G, L, and c. Still, a common concern with such non-linear formulations is the numerical stability of the estimation, i.e. how sensitive the inversion is to the input values. To address this, in the objective function we included a Sobolev term, which measures the magnitude of the gradient of the input-output map.[9,10] That is, we modified the original objective function to:

$$\hat{\omega} = \min_{\omega} ||x - f(\omega, b)||_2 + \lambda \cdot ||\nabla_b f(\omega, b)||_2 \tag{24}$$

where $\hat{x} = f(\omega, b)$ represents the inverse map from torso potentials to cardiac potentials (i.e. the inverse operator), and λ is left to the practitioner to adjust during the training phase. We note here that this is similar to but distinct from Total Variation (TV) regularization schemes, which are used to define unique solution by adding constraints on the sparsity or norm of the solution.[11] That is, in our formulation the Sobolev term guarantees stability of the inverse operator with respect to the input torso data, and was empirically found to be crucial to the training of the presented algorithm. These reconstruction results are discussed in the following section.

3. RESULTS

The proposed inversion method presented so far is predicated on having high quality training data measured in realistic environments and with accurate instrumentation. This requirement ensures that the inversion model learned by the network is representative of the physical relationship between body surface potentials and endocardial potentials. Accurate and precise instrumentation measurements of voltage potentials, however, require significant resources to produce. For this analysis, the data was acquired from an open source repository provided by the Consortium for Electro-Cardiographical Imaging (CEI) collected by professional medical researchers that study the biophysics of the heart. As a result, the experimental data was constrained in scope to the original study, however, the data source is available to the research community and could serve as a useful benchmark to compare against other methods available in the literature today.

In this section, the experimental setup and data collection methodologies are first briefly described. The description is followed by a presentation of the inversion results and discussion on the advantages and disadvantages of the proposed algorithm. Data visualizations and figures of merit are included here as well.

Downloaded From: https://www.spiedigitallibrary.org/conference-proceedings-of-spie on 3/11/2018 Terms of Use: https://www.spiedigitallibrary.org/terms-of-use

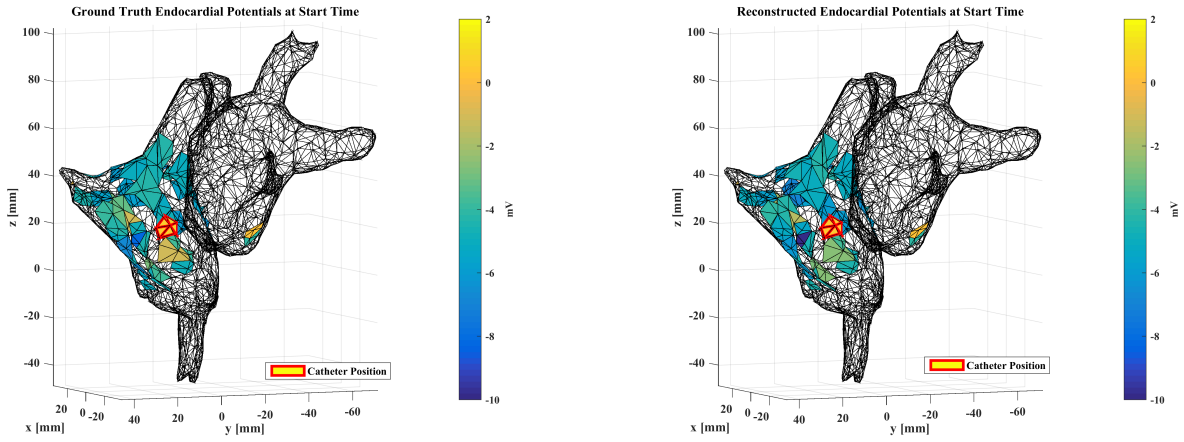
3.1 Experimental Setup

The open source data set was collected and curated by the Hospital General Universitario Gregorio Maran in Madrid, Spain as well as the Universitat Politcnica de Valncia Valencia, Spain.[12] The data-set was comprised primarily of two sets of electrical measurements of an atrial fibrillation patient undergoing medical care. The first set was composed of voltage potential measurements taken from the surface of the patient, and the second set had epicardial voltage potential measurements taken internally on the patient's atria. For the body surface potential measurements, 54 electrodes were placed at multiple spatial positions on the surface of the patients torso. The epicardial measurements were made using 62 electrodes that probed the atria of the heart through a precision catheter system. All of the voltage potential signals were measured simultaneously at a sampling rate of 2.03 kHz for a total duration of 7 seconds in length.

The objective of the study was to reconstruct epicardial potentials from only body surface potentials, as to aid in non-invasive ECGI medical diagnostics. Ideally, a larger spatial area would be measured for multiple patients for training, however, the experimentation was constrained to a small number of patients and sensors. Nonetheless the limited data collected with precise instrumentation still provides accurate electrical and spatial measurements that is critical to the data-driven approach proposed here.

3.2 Reconstruction Results

As discussed in Section 2, the objective of the proposed algorithm is to reconstruct the epicardial voltage potentials from only body surface potential measurements. In this effort, the model employed incorporates the body surface potential measurements as the input and epicardial voltages as the output. Given that both these measurements were recorded for the given data set, sufficient information was available to train a model to estimate this inverse function. However, because the spatial positioning of the measurements were fixed, the reconstruction results are limited to only the epicardial positions where the catheter probes were placed. With a larger data set acquired from multiple patients it may be possible to directly parameterize the model to incorporate different geometries, and even densely reconstruct 3D tissue profiles.



(a) Ground Truth Spatial Map Epicardial Potentials (b) Reconstructed Spatial Map of Epicardial Potentials

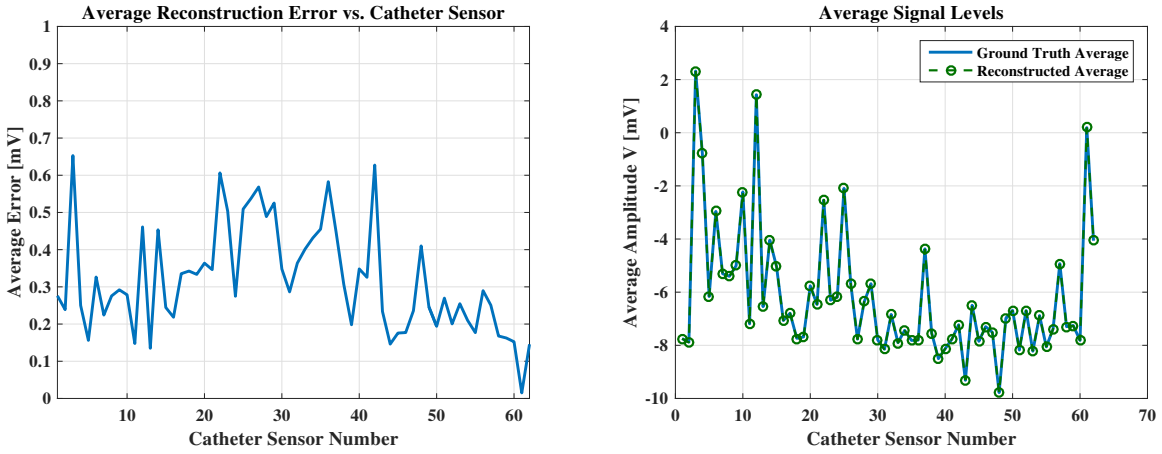
Figure 1: Spatial Reconstruction of Epicardial Potentials

In particular, for training the neural network only the measured data from one patient was considered. Concurrently, it was desirable to determine how the model would perform for data not specifically used to train the model. To achieve this with the limited data source, the body surface and epicardial measurements were separated into two disjoint sets. From the original data signals, time samples were randomly chosen to serve as the training data. After the training data was used to optimize the network, the remaining data was used to test the reconstruction accuracy. Because the time samples were chosen at random sample instances, this ensures time invariance for the learned inverse model.

Downloaded From: https://www.spiedigitallibrary.org/conference-proceedings-of-spie on 3/11/2018 Terms of Use: https://www.spiedigitallibrary.org/terms-of-use

The reconstructed potentials were mapped to the spatial position of the catheters measurements from the geometry provided in the dataset. This was visualized over a surface mesh with the full atria and heart's geometry to provide context and intuition on where the voltage potentials are concentrated. This visualization for a single instance in time can be seen in Fig. 1, where Fig. 1a and Fig. 1b respectively show the ground truth spatial distribution known from the experimental data and the reconstruction results produced by the inversion model. As can be seen, there is a strong correspondence between the reconstruction and ground truth results, which could aid clinicians in understanding epicardial potentials without having to perform invasive procedures.

The average reconstruction error for each sensor was also averaged across the entire time series, as can be seen in Fig. 2. Here the average error does not exceed 0.7mV over the various sensor positions, indicating that the reconstruction model does not suffer from any spatial bias. Therefore at any point in time, given body surface potential measurements, this model could be used to accurately reconstruct epicardial voltage potentials of the heart to within a prescribed tolerance.



(a) (b)

Figure 2: Average Reconstruction Error (a) and Average Signal Levels (b) vs Catheter Number

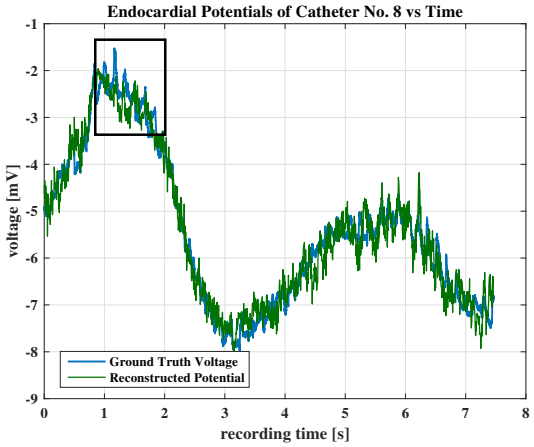
The performance of the reconstruction model was evaluated using several test statistics. The mean error, percentage error, and standard deviation of the estimator are displayed in Table 1. The average error over the entire test data set was found to be 0.312mV, which yielded a 12.59% relative error compared to the measured data. These results indicate that a high degree of confidence may be placed in the reconstruction of the epicardial potential distribution. As seen in Table 1, the training results are in line with the reconstruction results, indicating that the model is fairly robust to new test data and that it has not been over fitted to the training data, which is an important quality for any neural network approach.

	Mean Error [mV]	**% Error**	σ **[mV]**
Reconstruction Results	0.312	12.59%	0.321
Training Results	0.310	12.07%	0.321

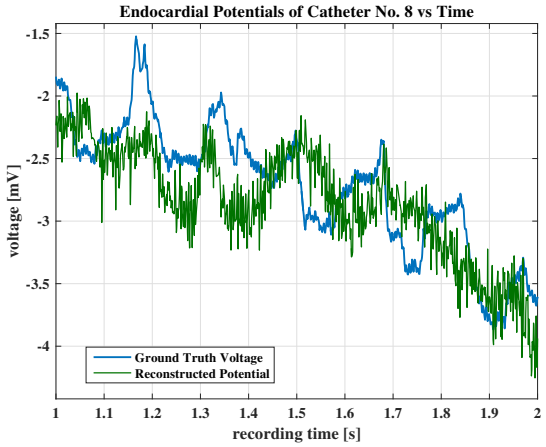
Table 1: Reconstruction Performance

Although the average error and percentage error are relatively low, some intuition into how the model reconstructs the signal can be seen in time plots of the epicardial potentials. Specifically the epicardial signal for Cahteter No. 8 can be seen in Fig. 3. For this signal plotted over all time, the reconstructed signal closely follows the general trend of the ground truth signal. However, when transient behavior is examined over a short period of time as shown in Fig. 3b, we see that the reconstruction signal does not closely track more subtle temporal features. Because there is no explicit time dependency in the model, it is limited in closely replicating

Downloaded From: https://www.spiedigitallibrary.org/conference-proceedings-of-spie on 3/11/2018 Terms of Use: https://www.spiedigitallibrary.org/terms-of-use



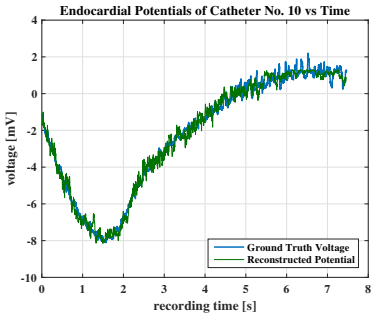
(a) Catheter No.8 Time Reconstruction



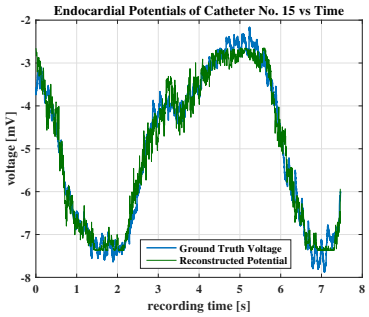
(b) Catheter No.8 Time Reconstruction Zoomed

Figure 3: Time Reconstruction of Epicardial Potential Signals

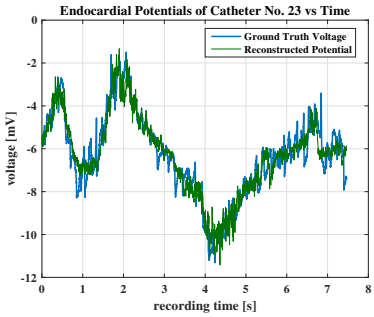
time-frequency behavior of epicardial signals. That is, although the spatial distribution of the epicardial potentials reconstructed with the model are fairly accurate on average, in our initial study small-signal temporal characteristics were not always faithfully recreated. For comparison, Fig. 4 below depicts the high-accuracy reconstruction results of several other catheter potentials, which agree with this analysis.



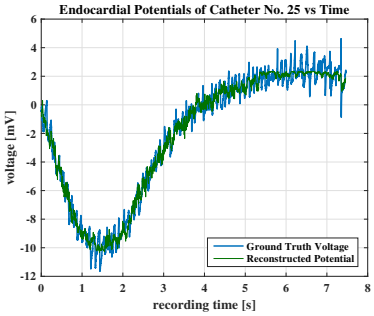
(a)



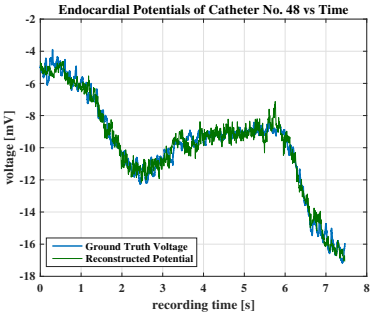
(b)



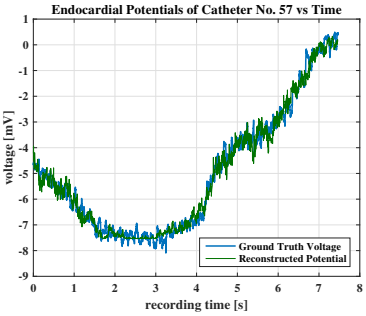
(c)



(d)



(e)



(f)

Figure 4: Time Reconstruction of Multiple Catheter Measurements

Downloaded From: https://www.spiedigitallibrary.org/conference-proceedings-of-spie on 3/11/2018 Terms of Use: https://www.spiedigitallibrary.org/terms-of-use

4. CONCLUSIONS

In summary, we have demonstrated the feasibility of a new data-driven approach for the non-invasive reconstruction and electronic imaging of human tissues. In particular, we have shown that it is possible to reconstruct interior epicardial potentials from body-surface ECG potentials to a high relative accuracy (∼88%) when the geometry is fixed or known. We believe our results show promise in the use of non-linear formulations of the inverse problem that can practically overcome some of the limitations posed by the linear Fourier theory, even when trained or optimized using simple gradient-based methods. One interesting feature of our approach is that the structure and functional form of the presented approximation networks are modeled and initialized based on the linear theory, which we believe aids in the ability for the simple gradient-based optimization methods to find desirable local minima. In future work, we plan to expand our study to incorporate frequency-dependent filters, cross-patient torso and cardiac geometries, and multi-modal imaging data such as MRI or CT into a single inversion model. In parallel, we continue to investigate universally convergent algorithms for finding robust solutions to polynomial systems of equations.

ACKNOWLEDGMENTS

The authors would like to thank the Air Force Research Laboratory for supporting this work under contract number FA8650-18-C-1137.

REFERENCES

[1] C. Mathers, *The global burden of disease: 2004 update*, World Health Organization, 2008.

[2] A. J. Shah, H. S. Lim, S. Yamashita, S. Zellerhoff, B. Berte, S. Mahida, D. Hooks, N. Aljefairi, N. Derval, A. Denis, *et al.*, "Non invasive ecg mapping to guide catheter ablation," *Journal of atrial fibrillation* **7**(3), 2014.

[3] Y. Rudy and H. Oster, "The electrocardiographic inverse problem.," *Critical reviews in biomedical engineering* **20**(1-2), pp. 25–45, 1992.

[4] C. Ramanathan, R. N. Ghanem, P. Jia, K. Ryu, and Y. Rudy, "Noninvasive electrocardiographic imaging for cardiac electrophysiology and arrhythmia," *Nature medicine* **10**(4), pp. 422–428, 2004.

[5] Y. Rudy, "Noninvasive ecg imaging (ecgi): Mapping the arrhythmic substrate of the human heart," *International Journal of Cardiology* **237**, pp. 13–14, 2017.

[6] B. J. Messinger-Rapport and Y. Rudy, "Computational issues of importance to the inverse recovery of epicardial potentials in a realistic heart-torso geometry," *Mathematical Biosciences* **97**(1), pp. 85–120, 1989.

[7] J. Nenonen and e. a. Horáček, B Milan, "Simulated epicardial potential maps during paced activation reflect myocardial fibrous structure," *Annals of Biomedical Engineering* **26**(6), pp. 1022–1035, 1998.

[8] A. Macovski, *Medical imaging systems*, Prentice Hall, 1983.

[9] S. Chandrasekaran, K. Jayaraman, J. Moffitt, H. Mhaskar, and S. Pauli, "Minimum sobolev norm schemes and applications in image processing," in *Proc. SPIE*, **7535**, 2010.

[10] S. Chandrasekaran and H. N. Mhaskar, "A minimum sobolev norm technique for the numerical discretization of pdes," *Journal of Computational Physics* **299**, pp. 649–666, 2015.

[11] J. Xu, A. R. Dehaghani, F. Gao, and L. Wang, "Noninvasive transmural electrophysiological imaging based on minimization of total-variation functional," *IEEE Transactions on Medical Imaging* **33**(9), pp. 1860–1874, 2014.

[12] J. Pedrón-Torrecilla, M. Rodrigo, A. M. Climent, A. Liberos, E. Pérez-David, J. Bermejo, A. Arenal, J. Millet, F. Fernández-Avilés, O. Berenfeld, *et al.*, "Noninvasive estimation of epicardial dominant high-frequency regions during atrial fibrillation," *Journal of Cardiovascular Electrophysiology* **27**(4), pp. 435–442, 2016.

Downloaded From: https://www.spiedigitallibrary.org/conference-proceedings-of-spie on 3/11/2018 Terms of Use: https://www.spiedigitallibrary.org/terms-of-use